Available online at www.sciencedirect.com
SCIENCE DIRECT®
Acta Materialia 52 (2004) 2837–2845
Acta MATERIALIA
www.actamat-journals.com

Three-dimensional phase-field simulations of coarsening kinetics of γ' particles in binary Ni–Al alloys

J.Z. Zhu [a,*], T. Wang [a], A.J. Ardell [b], S.H. Zhou [a], Z.K. Liu [a], L.Q. Chen [a]

[a] *Department of Materials Science and Engineering, Penn State University, 305 Steidle Building, University Park, PA 16802, USA*
[b] *Department of Materials Science and Engineering, University of California, Los Angeles, CA 90095, USA*

Received 20 January 2004; received in revised form 20 January 2004; accepted 25 February 2004
Available online 9 April 2004

Abstract

The coarsening kinetics of γ' precipitates in binary Ni–Al alloy is studied using three-dimensional (3D) phase-field simulations. The bulk thermodynamic information and atomic diffusion mobilities are obtained from databases constructed using the CALPHAD approach, while the experimental values for the interfacial energy, elastic constants and lattice mismatch are directly employed in the phase-field model. Specifically, we predict the morphological evolution, average precipitate size, and size distribution as a function of time for a given temperature and composition. Comparison of the phase-field simulation results with experiments shows good quantitative agreement in both time and length scales.

Keywords: Phase-field model; Ni-base alloys; Coarsening; Kinetics; Thermodynamics

1. Introduction

The typical microstructure of Ni-base alloys consists of a dispersion of ordered intermetallic precipitate particles of the type $L1_2$ (γ') coherently embedded in a matrix (γ) with a face-centered cubic (fcc) structure. The key to the successful development of superalloys is the control of the $\gamma' + \gamma$ two-phase microstructure and its high temperature stability, since the mechanical properties (e.g., strength, fatigue and creep) are strongly dependent on the γ' volume fraction, morphology and size distribution. Therefore, extensive efforts have been devoted to understanding the γ' precipitate evolution, both experimentally and theoretically, over the past fifty years [1].

There have been a number of attempts to model microstructural evolution and coarsening kinetics of ordered intermetallic γ' precipitates in Ni–Al alloys, particularly using the phase-field method (see, e.g., [2]). The phase-field method describes a microstructure using a set of conserved or non-conserved physical or artificial fields, and the microstructure evolution is predicted by numerically solving a set of mathematical equations governing the evolution of the fields. For example, Wang and Khachaturyan investigated the effect of elastic energy on the morphology of a single coherent precipitate during growth in two dimensions (2D) [3]. A composition field c and a single long-range order parameter field η were introduced to describe the $\gamma + \gamma'$ microstructure. The local free energy was approximated by a Landau-type of polynomial as a function of c and η. The coefficients in the free energy function were determined empirically to match the equilibrium compositions of the γ and γ' phases at a particular temperature. The evolution of the shape of a coherent γ' particle from a circle to a square was predicted to occur during its growth. To describe more physically the four types of antiphase domains that exist for the γ' precipitates as a result of the $L1_2$ type of ordering in the fcc lattice, a three-component long-range order parameter [4–6] was incorporated in the phase-field simulations [7–9], and the multi-particle effects, i.e., the elastic and diffusional interactions among precipitates, were studied [7,9]. Ex-

* Corresponding author. Tel.: +1-814-865-0389; fax: +1-814-865-2917.
E-mail address: zhu@ems.psu.edu (J.Z. Zhu).

1359-6454/$30.00 © 2004 Published by Elsevier Ltd on behalf of Acta Materialia Inc.
doi:10.1016/j.actamat.2004.02.032

perimentally observed morphological patterns, such as changes of the shape of the precipitates shape and their alignment along the elastically soft directions in the matrix, have been successfully predicted using 2D phase-field simulations. The effects of precipitate volume fraction on the coarsening kinetics were also modeled by Vaithyanathan and Chen [9] using 2D phase-field simulations and compared qualitatively with experimental measurements. The particle splitting process, i.e., one cuboidal particle splitting into two or more particles as a result of the coherent or an applied stress, was simulated in by Li and Chen (2D) [8], Banerjee et al. (2D) [10], and by Zhang et al. (3D) [11]. Recently Wen et al. [12] have shown that the formation of experimentally observed bimodal particle size distributions can be reproduced by 2D phase-field simulations under continuous cooling conditions. The results of 3D phase-field simulations of the morphological evolution of γ' precipitates have also been reported [13,14].

Despite the remarkable success of phase-field simulations in providing some fundamental understanding of the underlying thermodynamic and kinetic mechanisms leading to various morphological evolution of γ' precipitates, existing phase-field simulation results are largely qualitative due to the following reasons. First, most existing phase-field simulations of γ' precipitates in Ni-base alloys were carried out in 2D [3,7–10]. The very few 3D simulations of γ' precipitates are mainly concerned with the morphological evolution during precipitation rather than the quantitative description of growth and coarsening kinetics [13–15]. Secondly, in most of the existing phase-field simulations of γ' precipitate evolution, the local chemical free energy as a function of field variables was fitted only to the equilibrium compositions for a particular temperature [3,7–10,13,14], although there have been recent efforts to incorporate more realistic thermodynamic information, e.g., the chemical free energies of the γ and γ' phases from databases created by the CALPHAD approach [15]. Third, essentially all existing phase-field simulation results of γ' precipitate evolution were presented in reduced time unit. Finally, it has been shown that there is a limit to the length scale of a microstructure described by a phase-field model using the physical long-range order parameters [16]. As measured by atom-probe microscopy [17], the interfacial thickness between two solid phases is on the order of 1 nm, or at most 5 nm, depending on the system and temperature [18]. To resolve the diffuse-interface in the phase-field model, there must be a few grid points within the interface region to maintain numerical accuracy and stability. An estimate of the γ/γ' interface width in Ni–Al binary alloys showed that current phase-field models with existing numerical approaches and computing power were limited only to small systems, i.e., on the order of hundreds of nanometers to one micron in 2D or tens of nanometers in 3D [16]. Such a small size is not large enough for studying the late stages of the coarsening process in real 3D alloys, where a sufficient number of particles is required for good statistical measurements.

There are a number of approaches that may be explored to increase the physical size of a phase-field simulation cell. One approach is to employ a numerical technique that is based on adaptive meshing rather than the uniform grids used in all existing phase-field simulations of γ' precipitates. An adaptive method uses more grid points across an interface where the phase-field variables change dramatically than inside a domain or phase where the field variables are largely uniform. Although such an approach has been employed in modeling the growth morphology of a single dendrite in 2D [19] and 3D [20], it is not clear under what conditions, e.g., under what ratio of the total interfacial area to volume in a microstructure, it is advantageous to employ an adaptive mesh technique for the γ' morphology evolution during nucleation, growth and coarsening as compared to a uniform grid method such as the semi-implicit Fourier spectral method [21,22]. Another approach is to simply scale the time and spatial length of the results from phase-field simulations based on the known physics for a given process [23] or energetic contributions to the thermodynamics of a microstructure [15]. For example, the total surface energy is proportional to the total interfacial area whereas the total elastic energy is proportional to the precipitate volume. Increasing the elastic energy artificially is approximately equivalent to increasing the length scale of a system [15]. A third approach is to directly change the thermodynamic description of a phase-field model. A good example is the model proposed by Kim et al. [24] who have completely removed the actual chemical free energy contribution to the interfacial energy for an equilibrium interface and replaced it with a double-well potential. In this approach, all the order parameter fields are artificial fields and the interfacial thickness is a computational length scale rather than the physical thickness. Cha et al. [25] recently used this approach to model the morphology of a single γ' precipitate during growth using one composition field and one artificial order parameter field. They were able to predict the fascinating dendritic growth and subsequent splitting of a γ' particle with a length scale comparable to experimental observations. However, due to the 2D nature of the simulations, the simplified chemical free energy functions of γ and γ' as functions of composition, as well as the fact that no real time scale was presented in the result, the simulation result is a qualitative prediction of the possibility of dendritic growth and splitting in to four particles of a single coherent precipitate in 2D. More recently, Zhu et al. [16] adopted a similar thermodynamic description to investigate the temporal evolution of a single γ' particle in a supersaturated γ matrix. With the thermody-

namic and kinetic descriptions from the CALPHAD databases, the growth kinetics of a precipitate in 1D was predicted with real length and time scales, and the results are shown to be essentially the same as those obtained from DICTRA calculations with a sharp-interface model [26]. Since the phase-field simulations were performed in 1D, it is not possible to predict the morphological evolution and coarsening kinetics of γ' particles.

The purpose of this paper is to report our quantitative predictions of the coarsening kinetics of γ' precipitates in Ni–Al alloys using 3D phase-field simulations. The results are compared with experimental observations and measurements. To the authors' knowledge, the present work represents the first 3D phase-field simulations which predicted coarsening kinetics of γ' precipitates that are in quantitative agreement with experimental measurements in both real time and spatial scales.

2. Model description

As discussed in the introduction, the focus of this work is on the quantitative comparison on the coarsening kinetics of γ' precipitates between simulations and experiments. We adopted the thermodynamic description of interfaces proposed by Kim et al. [24] for modeling solidification microstructures, which allows one to artificially increase the length scale of a phase-field simulation.

To distinguish the four types of ordered domains of the γ' phase and the disordered γ phase in a binary Ni–Al alloy, we employed one composition field $c(\mathbf{r},t)$ and four artificial order parameter fields $\phi_i(\mathbf{r},t)$ $(i=1,2,3,4)$ to describe the γ' precipitate microstructures. Different from the well-defined physical order parameters which represent the ordering reaction and the associated relative displacement vectors [4–6], the order parameters introduced here do not have direct physical meaning other than distinguishing the precipitate and matrix phases. The total free energy of an inhomogeneous microstructure described by the field variables is then given by [27],

$$F=\int_V\left[f(c,\phi_i)+\frac{\varepsilon^2}{2}\sum_{i=1}^{4}(\nabla\phi_i)^2\right]\mathrm{d}V, \tag{1}$$

where ε^2 is the gradient energy coefficient of the order parameters. In this approach, the diffuse-interface region is regarded as a mixture of the precipitate phase and matrix phase with different compositions but with equal chemical potentials [24,25],

$$c=h(\phi_i)c^{\mathrm{p}}+[1-h(\phi_i)]c^{\mathrm{m}},\quad \frac{\partial f^{\mathrm{p}}}{\partial c^{\mathrm{p}}}=\frac{\partial f^{\mathrm{m}}}{\partial c^{\mathrm{m}}}, \tag{2}$$

where $h(\phi_i)$ is a continuous function with values between 0 and 1. f^{p} and f^{m} are the chemical free energies of the precipitate and matrix phases, respectively.

The Gibbs free energies of the γ phase (f^{m}) and γ' phase (f^{p}) as functions of composition at any given temperature were taken directly from the available CALPHAD database. For given c and ϕ_i, there exists a single solution pair of c^{p} and c^{m} that satisfies Eq. (2). However, since the databases use a non-linear description of the Gibbs free energy, it is computationally intensive to directly solve Eq. (2). For simplicity, we established a table of c^{p} and c^{m} pairs with the same chemical potential and then obtained the corresponding solution by searching the tabulated values that would satisfy Eq. (2). Another simplification is to approximate the free energies using parabolic functions whose first and second derivatives are imported from the thermodynamic databases. Eq. (2) can be easily solved with a parabolic approximation. From our test results, no significant difference was found for the solutions of c^{p} and c^{m} between the parabolic approximation and the table-search method. In this work, the parabolic approximation was used.

The local free energy density of the system $f(c,\phi_i)$ is written as [24,25]

$$f(c,\phi_i)=h(\phi_i)f^{\mathrm{p}}(c^{\mathrm{p}})+(1-h(\phi_i))f^{\mathrm{m}}(c^{\mathrm{m}})+wg(\phi_i)+e^{\mathrm{el}}, \tag{3}$$

where $g(\phi_i)$ is the double-well potential, w is the double-well potential height and e^{el} is the elastic energy density. The functions $h(\phi_i)$ and $g(\phi_i)$ are selected as,

$$h(\phi_i)=\sum_{i=1}^{4}\left[\phi_i^3(6\phi_i^2-15\phi_i+10)\right], \tag{4}$$

$$g(\phi_i)=\sum_{i=1}^{4}[\phi_i^2(1-\phi_i)^2]+\alpha\sum_{i=1}^{4}\sum_{j\neq i}^{4}\phi_i^2\phi_j^2. \tag{5}$$

These functions meet the requirement that the free energy has its local minima located at $(\phi_1,\phi_2,\phi_3,\phi_4)=(1,0,0,0)$, (0,1,0,0), (0,0,1,0), (0,0,0,1) and (0,0,0,0). Eq. (3) represents the free energy of the precipitate and matrix phases, respectively, at these equilibrium values of the order parameters.

In the diffuse-interface description, the interfacial free energy σ is the excess free energy due to the field variable inhomogeneities in the system [28]. The parameters ε in Eq. (1) and w in Eq. (3) can be related to the interfacial energy σ and the interface thickness 2λ through $\sigma=\varepsilon\sqrt{w}/3\sqrt{2}$ and $2\lambda=\alpha\sqrt{2}(\varepsilon/\sqrt{w})$ where α is a constant dependent on the definition of the interface thickness 2λ [24]. There is one degree of freedom in choosing either w or 2λ to fit the value of the interfacial energy σ obtained from experimental measurements. Therefore, one may choose a larger interfacial width than the actual physical width of the interface by

decreasing the depth of the double-well potential, thus increasing the length scale of a simulation.

The elastic energy contribution to the morphological evolution and coarsening kinetics of γ' particles can be obtained using the microelasticity theory [29–31]. There are three factors contributing to the elastic energy: (1) the lattice misfit between the different phases; (2) the elastic constant inhomogeneity; (3) externally applied stress. The effects of external stress and elastic constant differences between the phases on coarsening can be incorporated, in principle, into the phase-field model [32–34]. In this paper, no external stress was applied. For a binary Ni–Al alloy, the elastic constant difference between the γ and γ' phases in the temperature range from 300 to 1100 K is not more than 7% [35,36]. From our simulations on Ni–Al alloys, no obvious differences in the morphology were observed, with and without considering the effects of elastic inhomogeneity, if no external stress was applied. Therefore, for simplicity, homogeneous elastic constants were assumed.

To describe the lattice parameter difference between γ and γ' phases, we assumed that the lattice parameter a depends on the order parameters ϕ_i as

$$a(\phi_i) = a_{\mathrm{m}} + h(\phi_i) \cdot \Delta a, \tag{6}$$

where a_{m} is the lattice parameter of the matrix phase, Δa is the difference between the lattice parameters a_{p} and a_{m} of the precipitate and matrix phases ($\Delta a = a_{\mathrm{p}} - a_{\mathrm{m}}$), and $h(\phi_i)$ follows the same definition in Eq. (4). Eq. (6) represents the lattice parameters of the precipitate and matrix phases when the value of $h(\phi_i)$ equals 1 and 0, respectively. Such a description of lattice parameter variation in a γ and γ' two-phase microstructure is less physical than previous phase-field models which assumed compositional dependence of lattice parameters using, e.g., the Vegard's law. However, it is computationally more convenient since a compositional dependence of lattice parameters will complicate the solutions of Eq. (2). Furthermore, no significant difference was found from our tests on precipitate morphologies using either the compositional or order parameter dependency of lattice parameters. In the present formulation, the local stress-free strain ϵ^0_{kl}, which characterizes the lattice mismatch between the disordered reference solution and a phase with order parameters ϕ_i, can be written as

$$\epsilon^0_{kl} = \frac{a(\phi_i) - a_{\mathrm{m}}}{a_{\mathrm{m}}} = \epsilon_0 \delta_{kl} h(\phi_i), \tag{7}$$

where $\epsilon_0 = \Delta a / a_{\mathrm{m}}$ is the lattice misfit and δ_{kl} is the Kronecker-delta function. Assuming that there is no change of macroscopic shape or volume during the phase transformation, the elastic strain is written as the difference between the local strain $\delta\epsilon_{kl}$ and the stress-free strain ϵ^0_{kl},

$$\epsilon^{\mathrm{el}}_{kl} = \delta\epsilon_{kl} - \epsilon^0_{kl}, \tag{8}$$

where $\delta\epsilon_{kl} = \frac{1}{2}(\partial u_k/\partial r_l + \partial u_l/\partial r_k)$ and $\mathbf{u}$ is the local displacement field. The stress tensor σ_{ij} is related to the elastic strain tensor by the Hooke's law, i.e., $\sigma_{ij} = C_{ijkl}\epsilon^{\mathrm{el}}_{kl}$, where C_{ijkl} denotes the elastic constants. Using the local mechanical equilibrium condition ($\partial\sigma_{ij}/\partial r_j = 0$) and Eqs. (7) and (8), we obtain

$$C_{ijkl}\frac{\partial^2 u_k}{\partial r_j \partial r_l} = \sigma^0_{ij}\frac{\partial h}{\partial r_j}, \tag{9}$$

where u_k denotes the kth component of the elastic displacement and $\sigma^0_{ij} = C_{ijkl}\epsilon_0\delta_{kl}$. In a periodic system, Eq. (9) can be easily solved in Fourier space [29–31]. The elastic energy density e^{el} in Eq. (3) is then evaluated as $e^{\mathrm{el}} = \frac{1}{2}\sigma_{ij}\epsilon^{\mathrm{el}}_{ij}$ once the displacement field is solved.

The morphological evolution of γ' precipitates is obtained by solving the two sets of kinetic equations [24,28]:

$$\frac{\partial c}{\partial t} = \nabla \cdot \left(M \nabla \frac{\delta F}{\delta c} \right) = \nabla \cdot \left(M \nabla \frac{\partial f}{\partial c} \right), \tag{10}$$

$$\frac{\partial \phi_i}{\partial t} = -L\frac{\delta F}{\delta \phi_i} = L(\varepsilon^2 \nabla^2 \phi_i - \frac{\partial f}{\partial \phi_i}), \tag{11}$$

where t is the time, M is the diffusion mobility and L is the kinetic coefficient for order parameter relaxation. The diffusion mobility term M is related to the atomic mobilities of Ni and Al through $M = c_{\mathrm{Al}}c_{\mathrm{Ni}}(c_{\mathrm{Al}}M_{\mathrm{Ni}} + c_{\mathrm{Ni}}M_{\mathrm{Al}})$ where M_{Ni} and M_{Al} are obtained from the atomic mobility database of the fcc phase [37]. The determination of the parameter L in Eq. (11) is more difficult. Although L can be related to the interface mobility through a thin-interface analysis, the interface mobility is not known. However, it should be noted that an accurate value of L is not necessary in our particular study since the coarsening kinetics is diffusion-controlled. Therefore, we chose a value for L which ensures that the γ' precipitate evolution process is diffusion-controlled.

Nucleation of γ' from the supersaturated γ phase was explicitly introduced into the system at the beginning of a phase-field simulation using an approach similar to that described by Simmons et al. [38]. Periodic boundary conditions were assumed for Eqs. (10) and (11). A semi-implicit Fourier spectral method was used for numerically solving these two sets of equations [21,22].

3. Results and discussions

In our phase-field simulations described below, almost all the required modeling parameters are either taken from databases or obtained from experimental measurements. The Gibbs free energy and diffusion mobility were imported from the thermodynamic and kinetic databases. Experimentally measured values used in the simulation include the interfacial energy,

elastic constants and lattice mismatch. The only disposable quantitative parameter is the artificial interfacial width, which determines the unit grid length scale and correspondingly the maximum system size that can be handled. The choice of the kinetic coefficients for the order parameter fields was discussed in the previous section. The unit time step is chosen to maintain numerical accuracy and stability. For a given temperature and alloy composition, the morphological evolution pattern can be simulated with real length and time scales. Quantitative information, such as the coarsening rate constant and particle size distribution, can also be analyzed from the output of the field variable distributions.

3.1. Constraints on the selection of interface width

Since an artificial γ/γ' interface is adopted in this model, we have the freedom to choose a wider interface thickness than the actual physical width, while fitting the interfacial energy to the experimentally obtained value. The larger the interface width we choose, the larger the length and time scale we are able to deal with. However, there are two major factors that still limit the maximum interface width that can be used for a simulation. First, the typical precipitate size at the beginning of coarsening in binary Ni–Al alloys is approximately 10–15 nm [39]. To represent precipitates at the initial stage numerically (or any precipitate with a small size at a later stage) by at least several grid points, there must exist an upper limit to the unit grid size. Consequently, there is a limit to the interface width, since a few grid points are always needed in the diffuse-interface region to satisfy numerical accuracy. Second, a wider interface is more likely to accelerate the coalescence of neighboring particles, especially at a high volume fraction.

Fig. 1 shows the influence of two different interface widths on coalescence. Simulations were performed using a 2D square lattice with an initial configuration of two circular γ' particles with different radii in a γ matrix with a sharp-interface at a temperature of 1023 K. The whole system size is 512×512 nm with a unit grid size of 2 nm. Initially the radii of the larger and smaller circular particles are 64 and 48 nm, respectively. Values of the equilibrium composition and order parameters, representing the same type of domain, were assigned to both phases. Different values of the gradient energy coefficient ε^2 and double-well potential height w were used, but were fitted to the same interfacial energy σ in the two calculations shown in Fig. 1. The 2D composition contour plot, as well as the 1D composition profile across the middle of the two circles, are shown both for smaller (Fig. 1(a)) and larger (Fig. 1(b)) 2λ values at two evolution times, $t = 200$ s (dashed line) and $t = 4400$ s (solid line). The

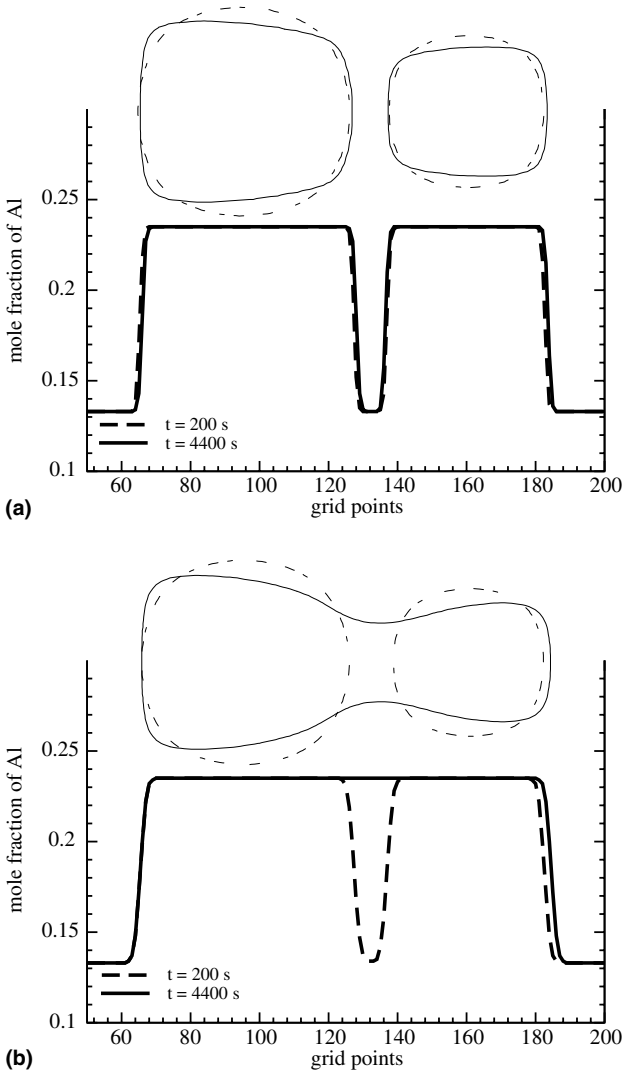

Fig. 1. Simulated evolution of two neighboring particles at two different γ/γ' interface widths 2λ. Shown are both 2D composition contours and 1D composition profiles at $t = 200$ s (dashed lines) and $t = 4400$ s (solid lines): (a) $2\lambda = 6$ nm; (b) $2\lambda = 10$ nm.

interface width in Fig. 1(b) is approximately 1.6 times as that in Fig. 1(a). The two particles gradually change their shapes due to elastic interactions. At $t = 4400$ s, the two neighboring particles in Fig. 1(b) become connected while in Fig. 1(a) they remain separated. It seems that a single particle is more likely to feel the presence of nearby particles when a larger interface thickness is used. Though the two particles in Fig. 1(a) eventually coalesced at the later time, $t = 11{,}800$ s, those with wider interfaces in Fig. 1(b) coalesced at a much earlier time. Therefore, increasing the interface width accelerates coalescence of neighboring particles due to increased mutual interaction. Our study shows that the length scale in the current model can be increased up to 10 times the physical length scale without significantly altering the coarsening behavior.

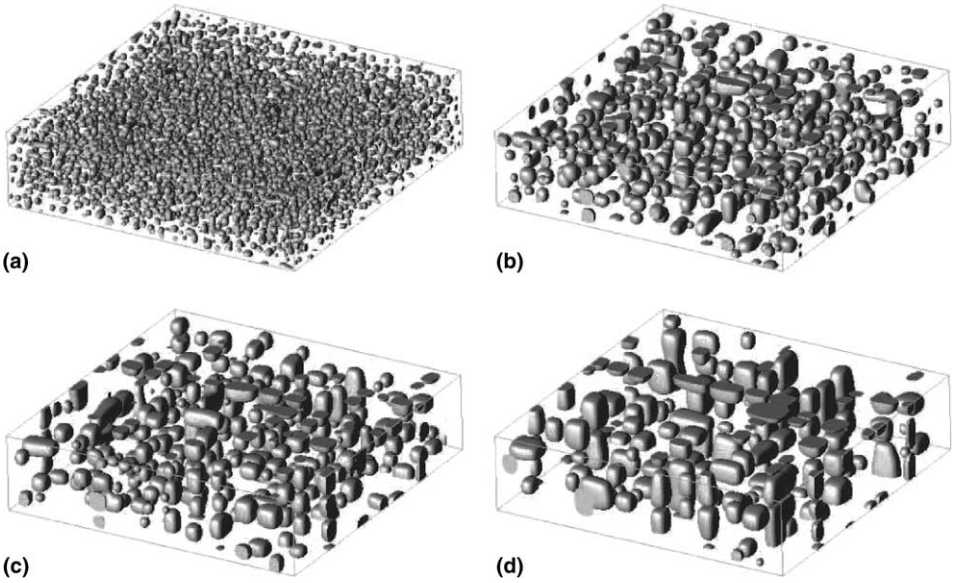

Fig. 2. Morphological evolution of γ' precipitates from 3D simulations in a Ni–13.8 at% Al alloy aged at 1023 K: (a) $t = 15$ min; (b) $t = 2$ h; (c) $t = 4$ h; (d) $t = 8$ h. Computational domain size is $160 \times 640 \times 640$ nm.

3.2. Morphological evolution

Fig. 2 shows the 3D morphological evolution of γ' precipitates in a Ni–13.8 at. %Al alloy at a temperature of 1023 K. The simulation was performed using a $64 \times 256 \times 256$ grid with a unit grid size of 2.5 nm. In other words, the system is $160 \times 640 \times 640$ nm in its physical size. The initial state was a homogeneous solution with small composition fluctuations around the average composition. Spherical nuclei with an average radius of 7.5 nm were randomly introduced to the computational domain at $t > 0$ where the mass balance must be maintained at all times. Approximately 6000 particles were formed during the nucleation stage. According to experimental observations [39], precipitation occurs very rapidly in this system. Thus we switched off the nucleation event at an early stage of aging ($t = 5$ min). Required input parameters, other than those directly taken from the thermodynamic and kinetic databases, are listed as follows: interfacial energy $\sigma = 0.01$ J/m^2 [40], elastic constants $C_{11} = 208$ GPa, $C_{12} = 148$ GPa, $C_{44} = 95.3$ GPa [35,36], lattice mismatch $\epsilon_0 = 0.00327$ [41], gradient energy coefficient $\varepsilon^2 = 6.0 \times 10^{-11}$ J/m and double-well potential height $w = 3.0 \times 10^7$ J/m^3.

The volume fraction of the γ' phase at the four different aging times in Fig. 2 is approximately 9–12%, which is very close to the equilibrium volume fraction of 10%. Precipitate coarsening is clearly seen in Fig. 2 where the number of particles in the computational domain reduces from about 2500 at $t = 15$ min to 110 at $t = 8$ h. Shrinking and growth of precipitates, as well as the coalescence of two neighboring domains, are observed. Driven by the reduction of the interfacial energy and elastic energy, the average precipitate size grows, accompanied by a change of particle shape from spherical to cuboidal, rod-like, or plate-like at later stages. The shape change from spheres to cubes occurs when the average particle size is around 20–25 nm at an aging time about 2–4 h, which is in good agreement with experimental observations [39].

We projected the simulated 3D particle distribution onto a 2D plane for comparison with experimental transmission electron microscope (TEM) images. The thin foils used in TEM measurements were typically from 20 to 120 nm thick in [39]. As shown in the left column of Fig. 3, we obtained 2D images projected from part of the 3D system, but with a thickness comparable to that of the experimental TEM samples. Experimental dark-field electron micrographs at the same aging time are also shown in the right column of Fig. 3 for comparison. All the morphologies shown in Fig. 3 are contained in a real physical area measuring 640×640 nm. The general morphological patterns obtained in the simulations agree well with those determined experimentally, particularly the precipitate shapes, alignment along the $\langle 100 \rangle$ crystallographic directions at later stages, and the particle densities.

3.3. Coarsening kinetics

Essentially all previous works on the coarsening kinetics of γ' precipitates indicated a cubic growth law for the increase in the average length scale. Since our emphasis in this work is on a quantitative comparison of the coarsening kinetics between the phase-field simulations and experiments, we use the same coarsening

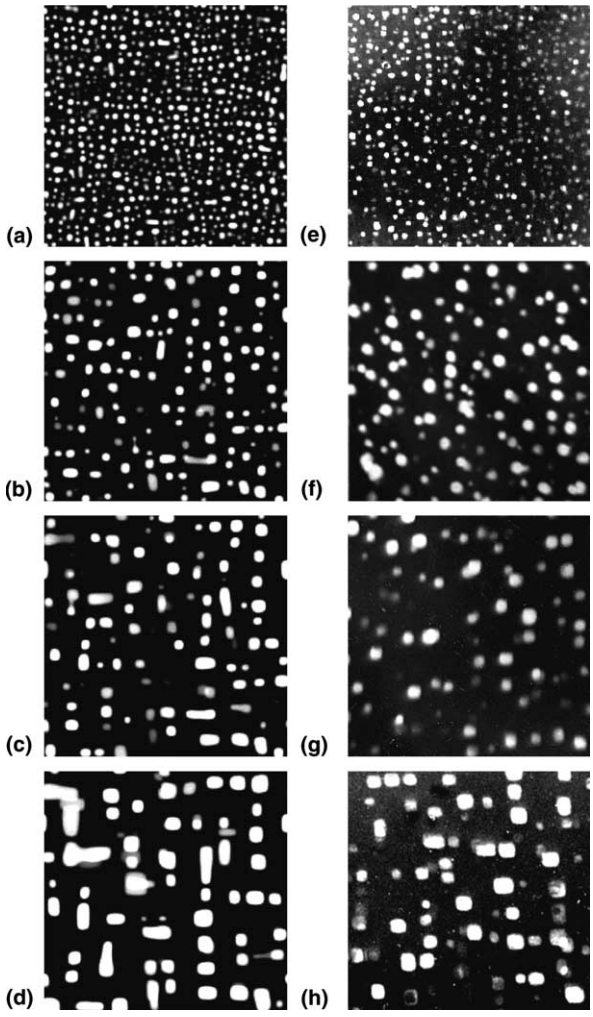

Fig. 3. Comparison of precipitate morphologies, projected in 2D (640×640 nm), obtained by simulations (left column) and experiments (right column) in a Ni–13.8 at% Al alloy aged at 1023 K: (a),(e) $t = 15$ min; (b),(f) $t = 2$ h; (c), (g) $t = 4$ h; (d), (h) $t = 8$ h. Sample thickness in experiments is from 20 to 120 nm, and in simulation is (a) 20 nm; (b) 40 nm; (c) 50 nm; (d) 80 nm.

exponent as that used in the experimental determination of coarsening rate constant [39]. For cube-shaped particles, the relationship between the average cube edge length $\bar{a}$ and aging time is expressed as

$$\bar{a}^3 - \bar{a}_c^3 = K(t - t_c), \tag{12}$$

where $\bar{a}_c$ and t_c are the average particle size and time at the beginning of coarsening, respectively. The constant K is known as the coarsening rate constant; it depends on the diffusion coefficient, interfacial energy and molar volume. To avoid the ambiguity in determining t_c, i.e., exactly when steady-state coarsening starts, we rewrite Eq. (12) as $\bar{a}^3 - \bar{a}_0^3 = Kt$, where $\bar{a}_0^3 = \bar{a}_c^3 - Kt_c$.

The mean particle edge length at different aging times was obtained by following the same procedures used in the experiments [39]. Fig. 4 shows the simulated and experimental results plotted as $\bar{a}^3 - \bar{a}_0^3$ vs. t on a logarithmic scale. The solid and dashed lines are linear fits to the data from the simulations and experiments, respectively. While the cubic growth law provided reasonably good fits observed in both cases, the data from the simulation seems to fit better than the experimental data. The experimentally determined values of the rate constant K and the initial particle size $\bar{a}_0$ are 4.60×10^3 nm^3/h and -2.99 nm, respectively [39]. From the solid line in Fig. 4, we obtained the values of K and $\bar{a}_0$ as 5.57×10^3 nm^3/h and -4.07 nm, respectively, indicating that the rate constant obtained from the simulations was approximately 20% higher than the experimentally determined one at the volume fraction.

There could be several factors causing the difference between the simulated and experimentally determined values of the rate constant. These include the interfacial energy, diffusion mobility, elastic constants and lattice mismatch used in the simulations. Systematic errors in the experimental measurements, e.g., the magnification calibration of the electron microscope, could also contribute to the discrepancy. It is highly possible that the interfacial energy and diffusion mobility used in the simulation differ from the real values by as much as 20%, or even 100% considering the large discrepancies that exist among reported values taken from the literature. In addition, the faster coalescence of neighboring particles in the simulations than in reality, due to the use of wider interface, may also lead to a higher rate constant. Given these considerations, the agreement between the rate constant obtained from the simulations and the experimentally measured value is excellent.

3.4. Particle size distributions

An important aspect of coarsening is dynamic scaling behavior, which means that the whole microstructure during steady-state coarsening is self-similar when scaled by the average length scale. Whereas the experimentally observed and simulated microstructures are never truly self-similar, the normalized particle size distributions (PSD) are typically time-invariant. The particle size distributions were measured by determining the fraction of particles of a given size that lie within specific size intervals, normalized by the average particle edge length. As mentioned earlier, there are more coalesced particles in the simulations than observed experimentally. It can be expected that more coalescence will shift the particle size distribution to larger sizes by broadening its tail. For comparison with experimental PSD results, we have excluded particles that might have coalesced if their aspect ratio is great than 3.

Fig. 5 shows the normalized PSD results obtained from the simulations (solid lines), experiments (dot-dashed lines) and the classical LSW theory [42,43]. The measured histograms were scaled so that the integral of the distribution, namely the total area under the histo-

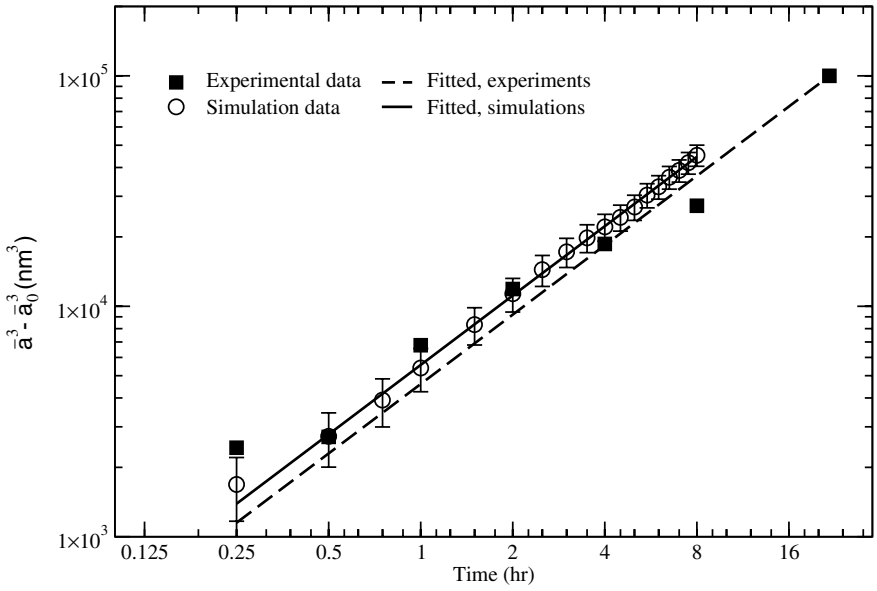

Fig. 4. Average length scale evolution plotted as $\bar{a}^3 - \bar{a}_0^3$ vs. t in a Ni–13.8 at% Al alloy aged at 1023 K.

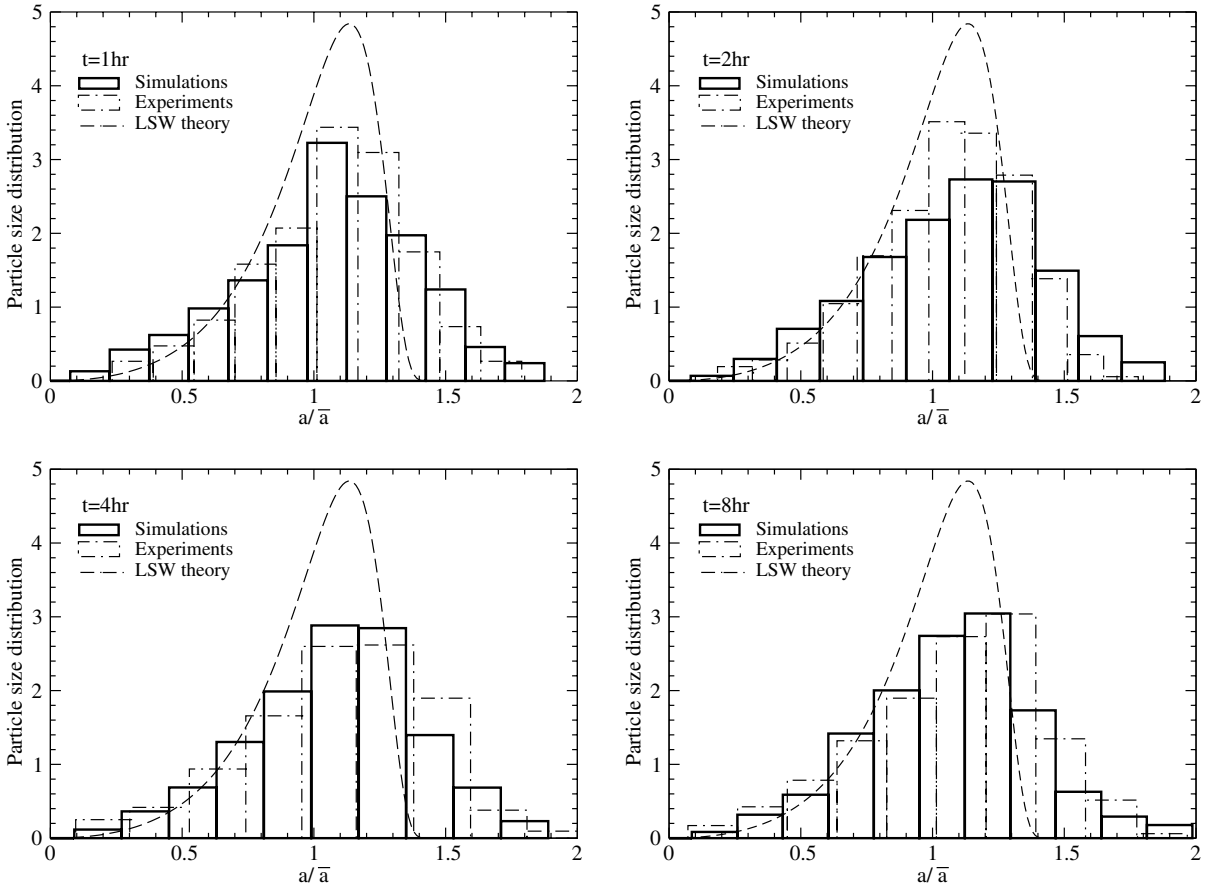

Fig. 5. Comparison of the particle size distributions obtained by simulations, experiments and the LSW theory in a Ni–13.8 at% Al alloy aged at 1023 K.

grams, is the same as the LSW theory, i.e., 9/4. The experimental data were taken from [39]. No obvious changes in the PSD shape were found at different times in both the simulations and experiments, implying that scaling behavior of the PSDs was observed during coarsening. The maxima in the simulations, as well as in

the experiments, are typically located at values of $a/\bar{a}$ of 1.05–1.3, as compared to the maximum at 1.135 in the LSW theory. Strictly speaking, the PSD predicted by the LSW theory holds only for spherical particles in an infinitesimally small volume fraction of dispersoids. With the particular volume fraction and particle shape considered, it is not surprising to see that the distributions in the simulations and experiments are both broader, with smaller maxima, than that predicted by the LSW theory. It is interesting to note that the size distributions obtained from the simulations agree quite well with those determined experimentally.

4. Summary

We have applied a 3D phase-field model to simulate the coarsening kinetics of γ' particles in Ni–Al alloys with real length and time scales. By artificially increasing the interfacial width, while keeping the interfacial energy constant, we were able to simulate microstructural evolution in physical systems with length and time scales comparable to experimental results. The simulated morphological pattern agrees well with experimental observations in terms of the particle density, morphology and spatial correlations. Good quantitative agreement was achieved between the simulations and experiments regarding the growth law, the coarsening rate constant, and the particle size distributions. The model developed is promising for quantitatively modeling and predicting microstructural evolution in commercial Ni-base superalloys.

Acknowledgements

The authors are grateful for the financial support from NASA under grant No. NCC3-920 and the computational resource award from NCSA under grant Nos. DMR030004N and DMR020002P. Simulations were performed in Pittsburgh Supercomputing Center and the LIONXL linux cluster supported partly by NSF-ITR under Nos. DMR-0205232, DMR-0122638, DMR-9983532 and DMR-9633719, as well as the Materials Simulation Center, a Penn-State MRSEC and MRI facility.

References

[1] Baldan A. J Mater Res 2002;37:2379.
[2] Chen LQ. Annu Rev Mater Res 2002;32:113.
[3] Wang Y, Khachaturyan AG. Acta Metall Mater 1995;43:1837.
[4] Lai ZW. Phys Rev E 1990;41:9239.
[5] Braun RJ, Cahn JW, McFadden GB, Rushmeier HE, Wheeler AA. Acta Mater 1997;46:1.
[6] Braun RJ, Cahn JW, McFadden GB, Wheeler AA. Philos Trans R Soc A 1997;355:1787.
[7] Wang Y, Banerjee D, Su CC, Khachaturyan AG. Acta Mater 1998;46:2983.
[8] Li DY, Chen LQ. Acta Mater 1999;47:247.
[9] Vaithyanathan V, Chen LQ. Acta Mater 2002;50:4061.
[10] Banerjee D, Banerjee R, Wang Y. Scr Mater 1999;41:1023.
[11] Zhang JD, Li DY, Chen LQ. Mat Res Soc Symp Proc 1998;481:243.
[12] Wen YH, Simmons JP, Shen C, Woodward C, Wang Y. Acta Mater 2003;51:1123.
[13] Rubin G, Khachaturyan AG. Acta Mater 1999;47:1995.
[14] Vaithyanathan V, Chen LQ. Mat Res Soc Symp Proc 2000;580:327.
[15] Zhu JZ, Liu ZK, Vaithyanathan V, Chen LQ. Scr Mater 2002;46:401.
[16] Zhu JZ, Wang T, Zhou SH, Liu ZK, Chen LQ. Acta Mater 2004;52:833.
[17] Blavette D, Bostel A, Sarru JM. Metall Trans A 1985;16:1703.
[18] Thornton K, Agren J, Voorhees PW. Acta Mater 2003;51:5675.
[19] Lan CW, Chang YC, Shih CJ. Acta Mater 2003;51:1857.
[20] Jeong JH, Goldenfeld N, Dantzig JA. Phys Rev E 2001;64:041602.
[21] Chen LQ, Shen J. Comput Phys Commun 1998;108:147.
[22] Zhu JZ, Chen LQ, Shen J, Tikare V. Phys Rev E 1999;60:3564.
[23] Shen C, Chen Q, Wen YH, Simmons JP, Wang Y. Scr Mater 2004;50:1023.
[24] Kim SG, Kim WT, Suzuki T. Phys Rev E 1999;60:7186.
[25] Cha PR, Yeon H, Yoon K. unpublished paper.
[26] Andersson JO, Helander T, Hoglund L, Shi PF, Sundman B. CALPHAD 2002;26:273.
[27] Wheeler AA, Boettinger WJ, McFadden GB. Phys Rev A 1992;45:7424.
[28] Cahn JW, Hilliard JE. J Chem Phys 1958;28:258.
[29] Khachaturyan AG. Theory of Structural Transformation in Solids. New York: Wiley; 1983.
[30] Khachaturyan AG, Shatalov GA. Sov Phys Solid State 1969;11:118.
[31] Chen LQ. In: Phase Transformations and Evolution in Materials. Warrendale, PA: TMS; 2000. p. 209.
[32] Hu SY, Chen LQ. Acta Mater 2001;49:1879.
[33] Zhu JZ, Chen LQ, Shen J. Model Simul Mater Sci Eng 2001;9:499.
[34] Wang YU, Jin YM, Khachaturyan AG. J Appl Phys 2002;92:1351.
[35] Prikhodko SV, Carnes JD, Isaak DG, Yang H, Ardell AJ. Metall Mater Trans A 1999;30:2403.
[36] Prikhodko SV, Carnes JD, Isaak DG, Ardell AJ. Scr Mater 1998;38:67.
[37] Engstrom A, Agren J. Z Metallkunde 1996;87:92.
[38] Simmons JP, Shen C, Wang Y. Scr Mater 2000;43:935.
[39] Ardell AJ, Nicholson RB. J Phys Chem Solids 1966;27:1793.
[40] Ardell AJ. Interface Sci 1995;3:119.
[41] Kamara AB, Ardell AJ, Wagner CNJ. Metall Mater Trans A 1996;27:2888.
[42] Lifshitz IM, Slyozov VV. J Phys Chem Sol 1961;19:35.
[43] Wagner CZ. Elektrochemistry 1961;65:581.